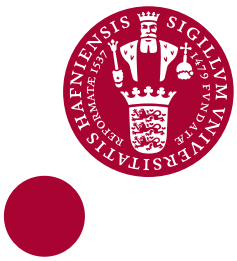

Reversal of Hypertriglyceridemia, Fatty Liver Disease, and Insulin Resistance by a Liver-Targeted Mitochondrial Uncoupler

Perry, Rachel J.; Kim, Taehan; Zhang, Xian-Man; Lee, Hui-Young; Pesta, Dominik; Popov, Violeta B.; Zhang, Dongyan; Rahimi, Yasmeen; Jurczak, Michael J.; Cline, Gary W.; Spiegel, David A.; Shulman, Gerald I.

Published in:
Cell Metabolism

DOI:
10.1016/j.cmet.2013.10.004

Publication date:
2013

Document version
Publisher's PDF, also known as Version of record

Cell Metabolism
Short Article

Reversal of Hypertriglyceridemia, Fatty Liver Disease, and Insulin Resistance by a Liver-Targeted Mitochondrial Uncoupler

Rachel J. Perry,[1,2,3] Taehan Kim,[4] Xian-Man Zhang,[1] Hui-Young Lee,[1,3] Dominik Pesta,[1] Violeta B. Popov,[2] Dongyan Zhang,[1] Yasmeen Rahimi,[1] Michael J. Jurczak,[2] Gary W. Cline,[1] David A. Spiegel,[4,5] and Gerald I. Shulman[1,2,3,6,*]
[1]Howard Hughes Medical Institute
[2]Department of Internal Medicine
[3]Department of Cellular & Molecular Physiology
[4]Department of Pharmacology
Yale University School of Medicine, New Haven, CT 06519, USA
[5]Department of Chemistry, Yale University, New Haven, CT 06520, USA
[6]The Novo Nordisk Foundation Center for Basic Metabolic Research, 2200 Copenhagen N, Denmark
*Correspondence: gerald.shulman@yale.edu
http://dx.doi.org/10.1016/j.cmet.2013.10.004

SUMMARY

Nonalcoholic fatty liver disease (NAFLD) affects one in three Americans and is a major predisposing condition for the metabolic syndrome and type 2 diabetes (T2D). We examined whether a functionally liver-targeted derivative of 2,4-dinitrophenol (DNP), DNP-methyl ether (DNPME), could safely decrease hypertriglyceridemia, NAFLD, and insulin resistance without systemic toxicities. Treatment with DNPME reversed hypertriglyceridemia, fatty liver, and whole-body insulin resistance in high-fat-fed rats and decreased hyperglycemia in a rat model of T2D with a wide therapeutic index. The reversal of liver and muscle insulin resistance was associated with reductions in tissue diacylglycerol content and reductions in protein kinase C epsilon (PKCε) and PKCθ activity in liver and muscle, respectively. These results demonstrate that the beneficial effects of DNP on hypertriglyceridemia, fatty liver, and insulin resistance can be dissociated from systemic toxicities and suggest the potential utility of liver-targeted mitochondrial uncoupling agents for the treatment of hypertriglyceridemia, NAFLD, metabolic syndrome, and T2D.

INTRODUCTION

Nonalcoholic fatty liver disease (NAFLD) is a key factor in the pathogenesis of type 2 diabetes (T2D) and affects one in three Americans (Petersen et al., 2005; Samuel and Shulman, 2012). NAFLD is also a key predisposing factor for the development of nonalcoholic steatohepatitis (NASH), cirrhosis, and hepatocellular carcinoma. Furthermore, it is anticipated that NAFLD-induced NASH will soon surpass hepatitis C and alcoholic cirrhosis as the most common indication for liver transplantation in the US (White et al., 2012). Therefore, new and effective therapies for treatment of NAFLD are urgently needed.

We hypothesized that a liver-targeted mitochondrial uncoupling agent might be an effective and safe approach for the treatment of NAFLD and insulin resistance by promoting the oxidation of hepatic triglyceride, while avoiding hyperthermia and associated systemic toxicities that typically occur with classic uncoupling agents. One of the best-characterized mitochondrial uncoupling agents is 2,4 dinitrophenol (DNP), a protonophore that shuttles protons across the mitochondrial membrane, dissipating the mitochondrial proton gradient and resulting in the conversion of the energy derived from mitochondrial substrate oxidation to heat. DNP was extensively used as a weight loss remedy in the 1930s but taken off the market by the FDA in 1938 due to the occurrence of fatal hyperthermia. Given that the toxicities of DNP are on-target effects related to systemic mitochondrial uncoupling, we hypothesized that the safety and therapeutic potential of DNP could be increased by targeting DNP to the liver. We therefore synthesized and screened liver-targeted DNP derivatives that would be preferentially metabolized by liver and converted to DNP. In this screen, we found that DNP-methyl ether (DNPME) both prevented and reversed nonalcoholic fatty liver disease, insulin resistance, and hyperglycemia in rat models of NAFLD and T2D without hepatic or renal toxicity.

RESULTS AND DISCUSSION

We hypothesized that targeting DNP to the liver would reduce hypertriglyceridemia, hepatic lipid content, and improve insulin sensitivity, without DNP-associated toxicities. We therefore generated several derivatives of DNP, which we hypothesized would be preferentially metabolized by the cytochrome P450 system in the liver to the active protonophore, DNP, and we screened them in isolated hepatocytes for their ability to increase oxygen consumption (Figures S1A and S1B available online). From this screen, we identified two compounds that raised oxygen consumption rates in plated hepatocytes with similar potencies to DNP. We selected DNPME for further in vivo studies due to its stability under acidic conditions, which would potentially allow oral administration. In contrast to DNP, which caused

a large, dose-dependent increase in rectal temperatures and rapid dose-dependent mortality at doses above 10 mg/kg, DNPME caused no such effects up to 200 mg/kg (Figures 1A–1D). Thus, we found that the 50% lethal dose (LD_{50}) of DNPME was almost 10-fold higher than that of DNP (Figure 1E). Daily treatment with DNPME for 5 days caused no appreciable hepatic or renal toxicity at daily doses below 50 mg/kg (Figures 1F–1I), but daily doses above 2.5 mg/kg were effective at reducing hepatic triglyceride accumulation in rats fed a high-fat diet and sucrose-supplemented (5%) drinking water (Figure 1J). In contrast, the toxic threshold of chronic DNP treatment was determined to be 1 mg/kg, whereas the lowest dose that was effective at lowering liver triacylglycerol (TAG) was 5 mg/kg (Figures S1C–S1G); thus, the ratio of effective-to-toxic dose for DNP was 0.2 compared to 10 for DNPME. From these data, we found that DNPME had a favorable therapeutic index (lethal dose for 50% of the population [LD_{50}]/minimum effective dose for 50% of the population [ED_{50}]) of 70, which compares favorably with other drugs that are in common use, such as acetaminophen, which has a LD_{50}/ED_{50} of 13. We selected the lowest effective daily dose of DNPME (5 mg/kg) to further characterize its effects in vivo. Daily treatment at this dose for 6 weeks caused no differences in liver or renal function tests, liver or renal histology, or rectal temperature (Figures 1K–1N, S1J, and S1K).

The safety and efficacy profiles of DNPME led us to examine whether DNPME treatment could reverse preexisting hypertriglyceridemia, hepatic steatosis, and insulin resistance in a rat model of NAFLD. To this end, we induced hepatic steatosis in rats by feeding them a high-fat diet with sucrose-supplemented drinking water, then treated them with DNPME or vehicle daily for 5 days. The rats treated with DNPME had lower fasting plasma glucose, triglyceride, and insulin concentrations compared to the vehicle-treated animals (Figures 2A–2C), despite identical body weight and food intake during the treatment period (Figures S2A and S2B). Consistent with the reduced fasting plasma glucose and insulin concentrations, DNPME-treated rats had a 20% reduction in basal endogenous glucose production (Figure 2D) and were much more glucose tolerant, as reflected by 30%–70% reductions in plasma glucose and insulin concentrations at each time point of an intraperitoneal (i.p.) glucose tolerance test (Figures 2E, 2F, S2C, and S2D). DNPME-treated rats also manifested increased whole-body insulin responsiveness as reflected by a greater than 3-fold increase in the glucose infusion rate required to maintain euglycemia during a hyperinsulinemic-euglycemic clamp (Figures 2G and S2E–S2G). This increase in insulin-stimulated whole-body glucose metabolism in the DNPME-treated rats could be attributed to improvements in both hepatic and peripheral insulin sensitivity (Figures 2H–2J). These improvements in hepatic and peripheral insulin sensitivity were associated with 40%–50% reductions in liver and muscle TAG (Figures 2K and 2L) and diacylglycerol (DAG) content (Figure S2H–S2K). Consistent with the reduced liver and muscle DAG concentration, we observed reduced protein kinase C epsilon (PKCε) and PKCθ translocation in liver and muscle, respectively, in DNPME-treated rats (Figures S2L and S2M), which is consistent with a role for DAG-mediated novel protein kinase C (nPKC) activation in causing the liver and muscle insulin resistance (Griffin et al., 1999; Yu et al., 2002; Itani et al., 2002; Samuel et al., 2004, 2007). In contrast, there were no differences in liver or muscle ceramide content, liver glycogen content, plasma adiponectin, FGF-21, or lactate concentrations, thus dissociating these factors from DNPME-induced improvements in liver and muscle insulin sensitivity in these animals (Figures S2N–S2S). We also examined the effect of DNPME on plasma markers of inflammation and found no effect of DNPME on any of these cytokines other than a small reduction in plasma interleukin-13 (IL-13) concentrations (Figure S2T).

In the context of the observed reductions in muscle TAG and DAG content and increases in skeletal muscle insulin sensitivity observed with DNPME treatment, we examined whether these effects of DNPME to lower muscle TAG and DAG content might be explained by DNPME-induced reductions in hepatic very-low-density lipoprotein (VLDL) production. Consistent with this hypothesis, we observed a 50% reduction in hepatic VLDL production with DNPME treatment (Figure 2M). In order to verify that DNPME treatment reduced hepatic TAG/DAG content by promoting increased hepatic mitochondrial uncoupling in vivo, we measured liver-specific rates of oxidative flux pathways and observed a 50% increase in rates of hepatic tricarboxylic acid cycle flux (V_{TCA}) (Figure 2N) after 1 and 5 days of DNPME treatment. This increased hepatic mitochondrial V_{TCA} flux was fueled entirely by increased hepatic fatty acid oxidation flux on day 1 when liver fat content was unchanged between vehicle- and DNPME-treated rats (18.2 ± 1.5 versus 16.9 ± 2.8 mg/kg, $p = 0.70$) but changed to an increase in mostly glucose oxidation, through increased pyruvate dehydrogenase flux (V_{PDH}) on day 5, when liver fat content normalized. This pyruvate dehydrogenase flux (V_{PDH})/V_{TCA} flux observed on day 5 was similar to that observed in the liver of normal chow-fed rats, whereas V_{PDH}/V_{TCA} flux on days 0 and 1 was consistent with that of high-fat-fed rats (Alves et al., 2011). Consistent with the reduced fasting plasma glucose concentrations and basal rates of hepatic glucose production in DNPME-treated rats after 5 days, these animals also exhibited a 30% reduction in hepatic pyruvate carboxylase flux (V_{PC}) (Figure 2O), whereas there was no difference in V_{PC} flux on the first day of DNPME treatment when liver TAG content was unchanged. In contrast, the ratio of mitochondrial fatty acid oxidation to V_{TCA} flux was unchanged by DNPME treatment in all other tissues, including skeletal muscle (Figure 2P). While these relative flux measurements do not allow us to rule out a small absolute increase in V_{TCA} in peripheral tissues, they are consistent with the hypothesis that the functional effects of DNPME to raise oxygen consumption rate in vivo are limited mostly to the liver.

Given the effects of DNPME to reduce ectopic lipid content in liver and skeletal muscle and improve whole-body insulin sensitivity in both the NAFLD prevention and reversal studies, we examined whether DNPME treatment would improve fasting and postprandial plasma glucose and insulin concentration profiles in a rat model of T2D. To evaluate this question, we examined the effect of 14 days of DNPME versus vehicle treatment in a high-fat-fed and STZ-nicotinamide-treated rat model of T2D (Masiello et al., 1998; Reed et al., 2000; Samuel et al., 2004). Despite having no difference in body weight or white adipose tissue (WAT) weight, and consistent with a primarily hepatic uncoupling effect and unchanged whole-body metabolism (Figures S3A and S3B), DNPME treatment normalized fasting

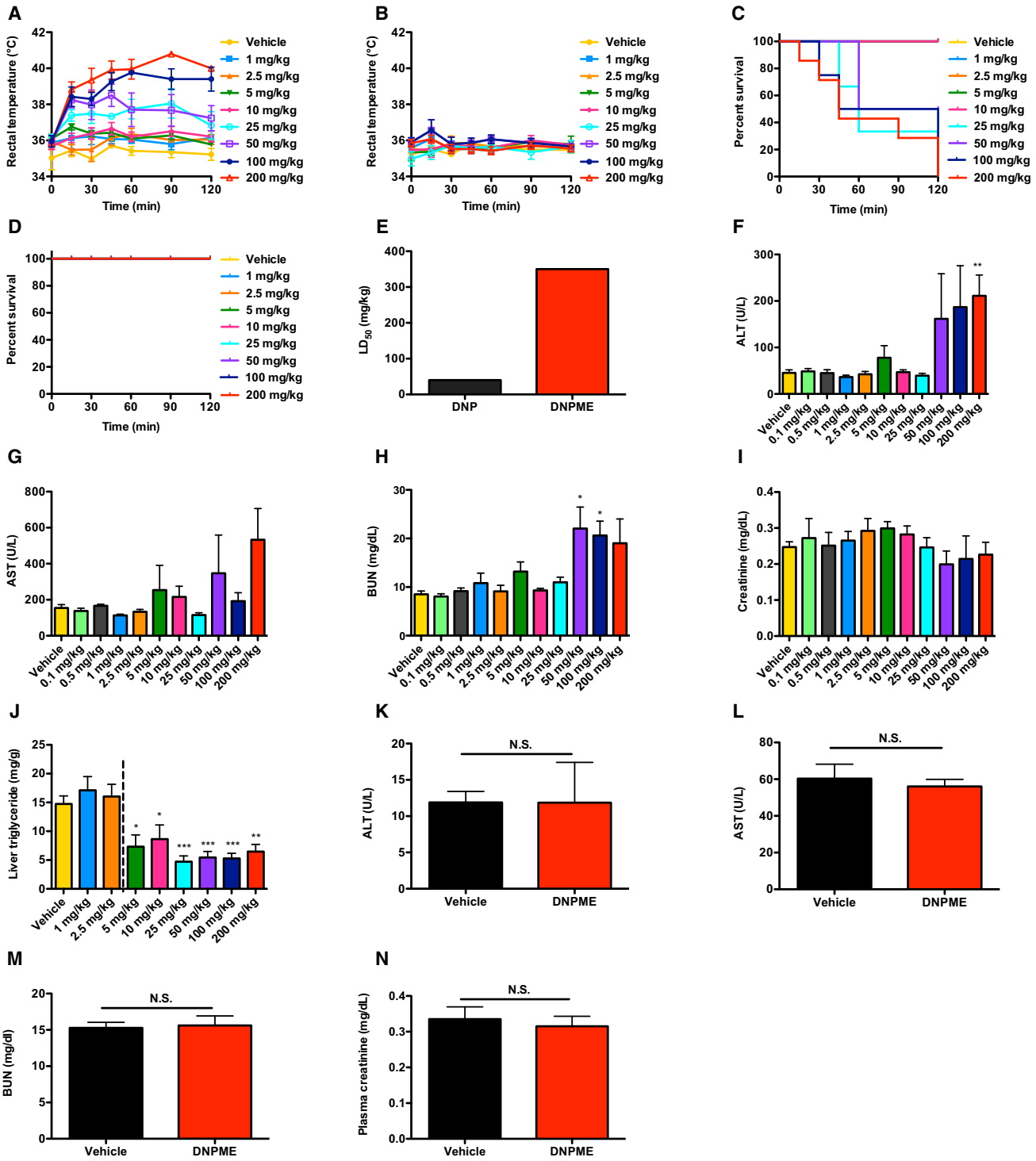

Figure 1. Safety and Efficacy Profile of DNPME and DNP in Rats

(A and B) Rectal temperature following a single i.p. injection of DNP (A) or DNPME (B).

(C and D) Survival acutely following treatment with DNP (C) or DNPME (D).

(E) LD_{50} of DNP and DNPME.

(F–I) Plasma ALT (F), AST (G), BUN (H), and creatinine (I) after 5 days of daily treatment with DNPME or vehicle in chow-fed rats.

(J) Liver TAG in overnight-fasted rats after 5 days of daily treatment with DNPME during high-fat/sucrose water feeding.

(K–N) Liver and renal function tests: ALT (K), AST (L), BUN (M), and creatinine (N) after 6 weeks of daily DNPME treatment (5 mg/kg) in chow-fed rats. For all panels, n = 4–6 per dose, and data are represented as mean ± SEM. See also Figure S1.

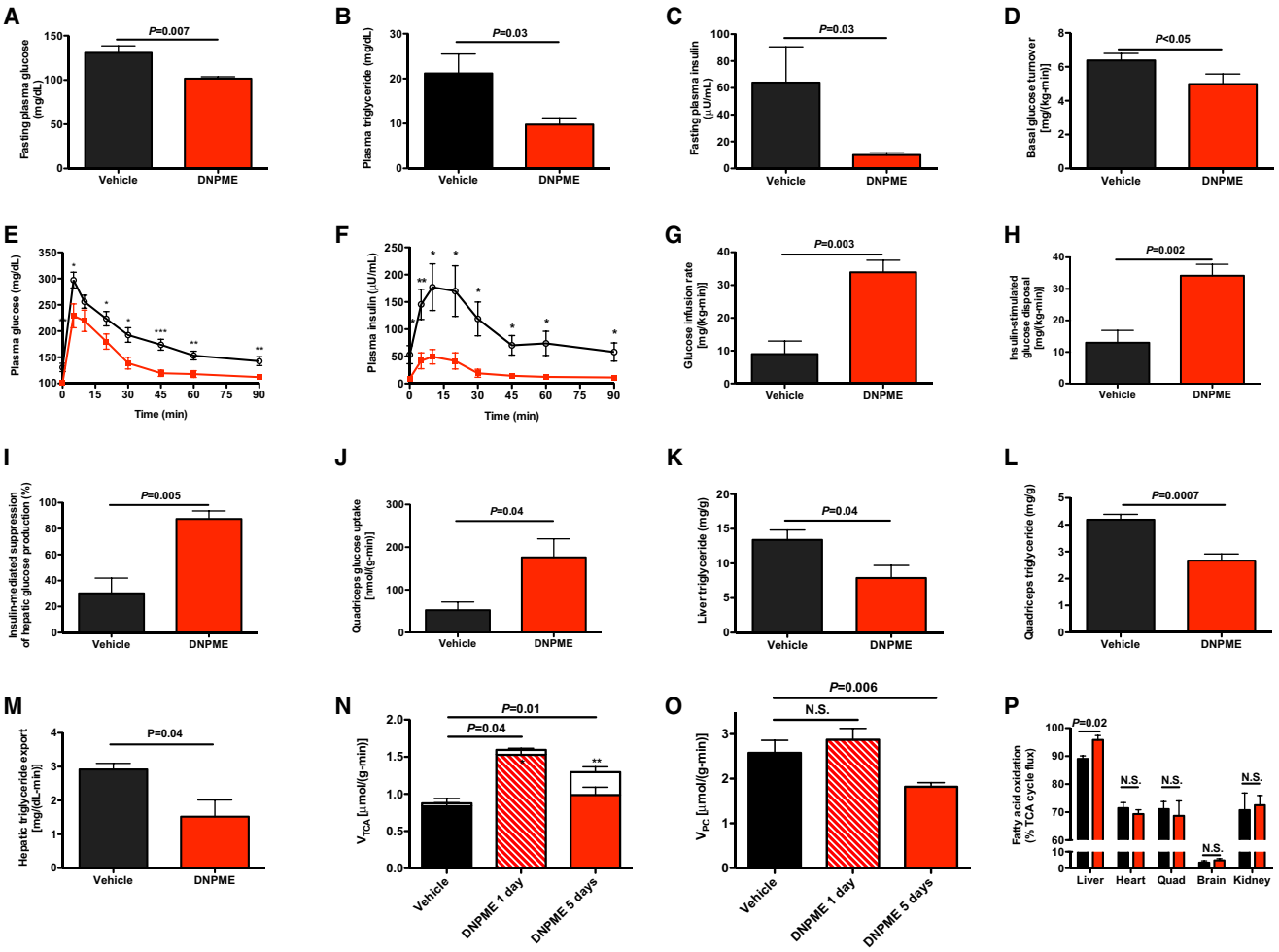

Figure 2. DNPME Reverses NAFLD, Hypertriglyceridemia, and Liver and Muscle Insulin Resistance in Rats Fed High-Fat Diet and Sucrose Water for 2 Weeks, then Treated with 5 mg/kg DNPME per Day for 5 Days

(A–C) Fasting plasma glucose (A), triglyceride (B), and insulin (C).

(D) Basal glucose turnover.

(E and F) Plasma glucose (E) and insulin (F) during an i.p. glucose tolerance test. Black circles, vehicle treated; red squares, DNPME treated. *$p < 0.05$, **$p < 0.01$, ***$p < 0.001$.

(G) Glucose infusion rate to maintain euglycemia during the hyperinsulinemic-euglycemic clamp.

(H) Insulin-stimulated glucose metabolism.

(I) Insulin-mediated suppression of hepatic glucose production.

(J) Insulin-stimulated glucose uptake in quadriceps.

(K and L) TAG in liver (K) and quadriceps (L).

(M) Liver VLDL production.

(N) Liver TCA cycle flux (sum of red and white bars) and substrate contributions (fatty acid oxidation, solid bar; PDH flux, white bar) to the TCA cycle. n = 3 vehicle treated, 3 DNPME treated for 1 day, and 6 DNPME treated for 5 days.

(O) Hepatic flux through pyruvate carboxylase. Rats were fasted overnight prior to each of these studies.

(P) Fatty acid oxidation (% V_{TCA}) in 1 day DNPME or vehicle-treated rats. Unless otherwise specified, n = 5–8 per group. Data are mean ± SEM. n = 3 vehicle treated, 3 DNPME treated for 1 day, and 6 DNPME treated for 5 days. See also Figure S2.

plasma glucose and triglyceride concentrations (Figures 3A–3C). DNPME treatment also resulted in a marked improvement in glucose tolerance associated with lower plasma insulin concentrations, reflecting improved whole-body insulin sensitivity (Figures 3D, 3E, S3C, and S3D). Finally, and consistent with the results in the other insulin-resistant rodent models of NAFLD, DNPME treatment caused a marked reduction in both liver and muscle TAG content (Figures 3F and 3G), without any indication of renal or hepatic histopathology (Figures S1E and S1F). To further test the assertion that DNPME treatment ameliorates hyperglycemia in a rat model of chronic type 2 diabetes, we performed 5-day DNPME treatment studies on Zucker Diabetic Fatty rats concurrently fed a high-fat diet and sucrose-supplemented drinking water. Similar to the results in the T2D model previously described, DNPME treatment resulted in reductions in fasting plasma glucose, insulin, and liver triglyceride

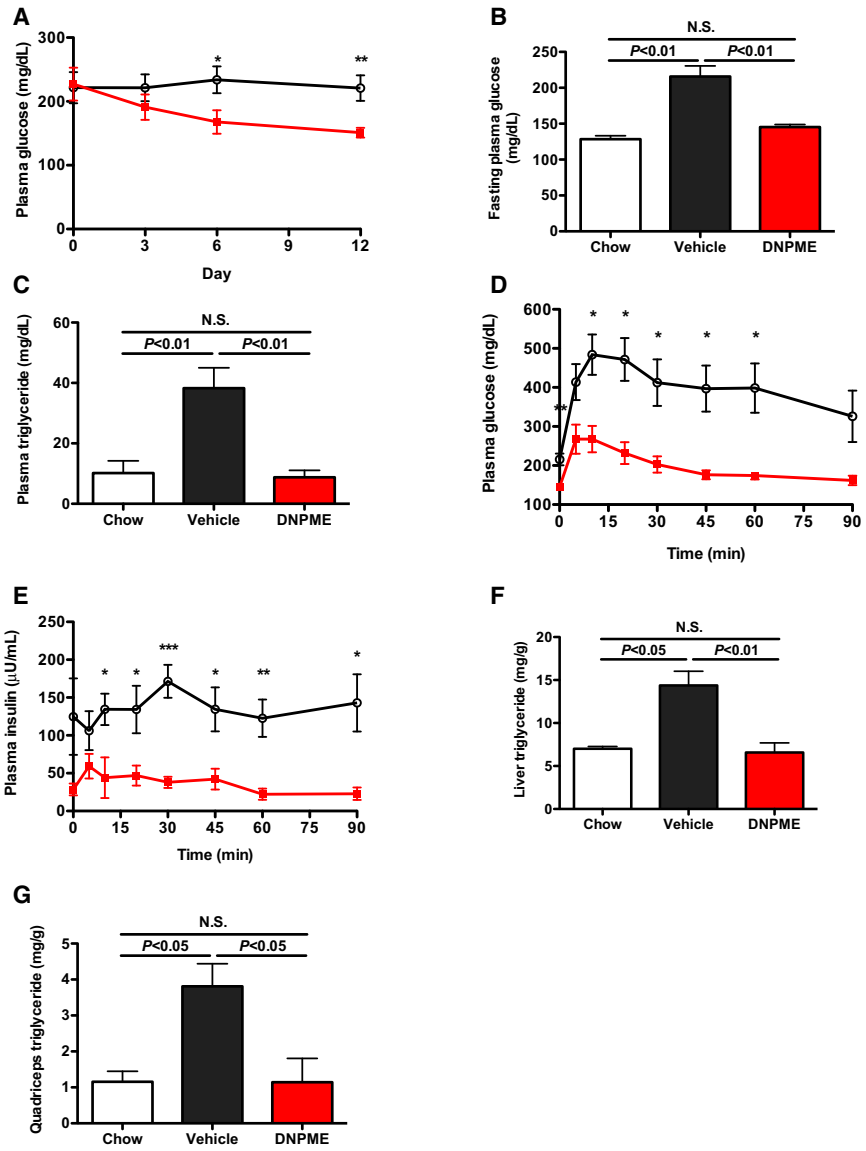

Figure 3. Daily 5 mg/kg DNPME Reverses Hyperglycemia, Hypertriglyceridemia, and Hepatic Steatosis in a Low-Dose-Streptozotocin-Treated, 3-Day High-Fat-Fed Rat Model of Type 2 Diabetes

(A) Random plasma glucose concentrations during DNPME treatment.

(B and C) Fasting plasma glucose (B) and TAG (C).

(D and E) Concentrations of plasma glucose (D) and insulin (E) in an intraperitoneal glucose tolerance test.

(F and G) TAG in liver (F) and quadriceps (G). For all panels, n = 4–7 per group. Rats were fasted overnight before each study. Data are represented as mean ± SEM. In the panels comparing chow, vehicle-treated, and DNPME-treated rats, comparisons were by ANOVA. See also Figure S3.

concentrations, with no indication of liver or renal dysfunction (Figures S3G–S3O).

In order to examine the impact of DNPME on whole-body energy expenditure and other metabolic parameters, we performed metabolic cage studies in DNPME- and vehicle-treated mice. Interestingly, we observed no effects of DNPME (5 mg/kg per day) on whole-body oxygen consumption, carbon dioxide production, energy expenditure, respiratory quotient, or activity (Figures S4A–S4E). Consistent with the rat studies, we also observed no effect of DNPME on food intake (Figure S4F). Taken together, these data suggest that DNPME at a dose of 5 mg/kg per day promotes subtle increases in hepatic energy uncoupling that can result in major reductions in liver and muscle fat content with associated reversal of liver and muscle insulin resistance without a major impact on whole-body energy expenditure.

It is also possible that low circulating levels of DNP, derived from hepatic conversion of DNPME to DNP by the P450 system, promote low levels of mitochondrial uncoupling in muscle and other extrahepatic organs. In order to examine this possibility, we assessed the effects of DNPME and DNP on state 4 oxygen consumption in vitro and observed an increase in oxygen consumption of liver, but not brain, by DNPME, whereas DNP promoted increased state 4 mitochondrial oxygen consumption in isolated mitochondria in both tissues. In contrast, neither drug uncoupled skeletal or cardiac muscle or kidney at the tissue concentrations measured in the DNPME-treatment studies (Figures S4G–S4K). These data imply that at the dose of DNPME administered in vivo, the mitochondrial uncoupling effect of DNPME appears to be mostly restricted to the liver and can be attributed to local conversion of DNPME to DNP by the P450 system. These data are consistent with the observed selective effect of DNPME to only increase mitochondrial fat oxidation flux/V_{TCA} flux in liver (Figure 2P) and the higher DNP concentrations in liver relative to skeletal muscle, heart, and brain following DNPME treatment (Figure 4C). While kidney DNP concentrations were similar to liver, this could be attributed to the fact that DNP is cleared from the body mostly by renal excretion. It is also possible that there was some renal conversion of DNPME to DNP due to the presence of P450 in the kidney. However, in contrast to liver, we did not observe any effects of DNPME to increase mitochondrial fat oxidation flux/V_{TCA} flux in kidney, suggesting minimal effects of DNPME on renal mitochondrial function in vivo. In addition, we observed no differences in ATP/AMP, ATP/ADP, or NADH/NAD^+ ratios in liver and skeletal muscle or in phosphorylation of hepatic AMP-activated protein kinase (AMPK) or its downstream target acetyl coenzyme A (CoA) carboxylase (ACC), demonstrating that DNPME is not altering the intracellular energy charge in these tissues at this therapeutic dose (Figures S4L–S4R); however, we cannot rule out a small effect on peripheral tissues from either local DNPME

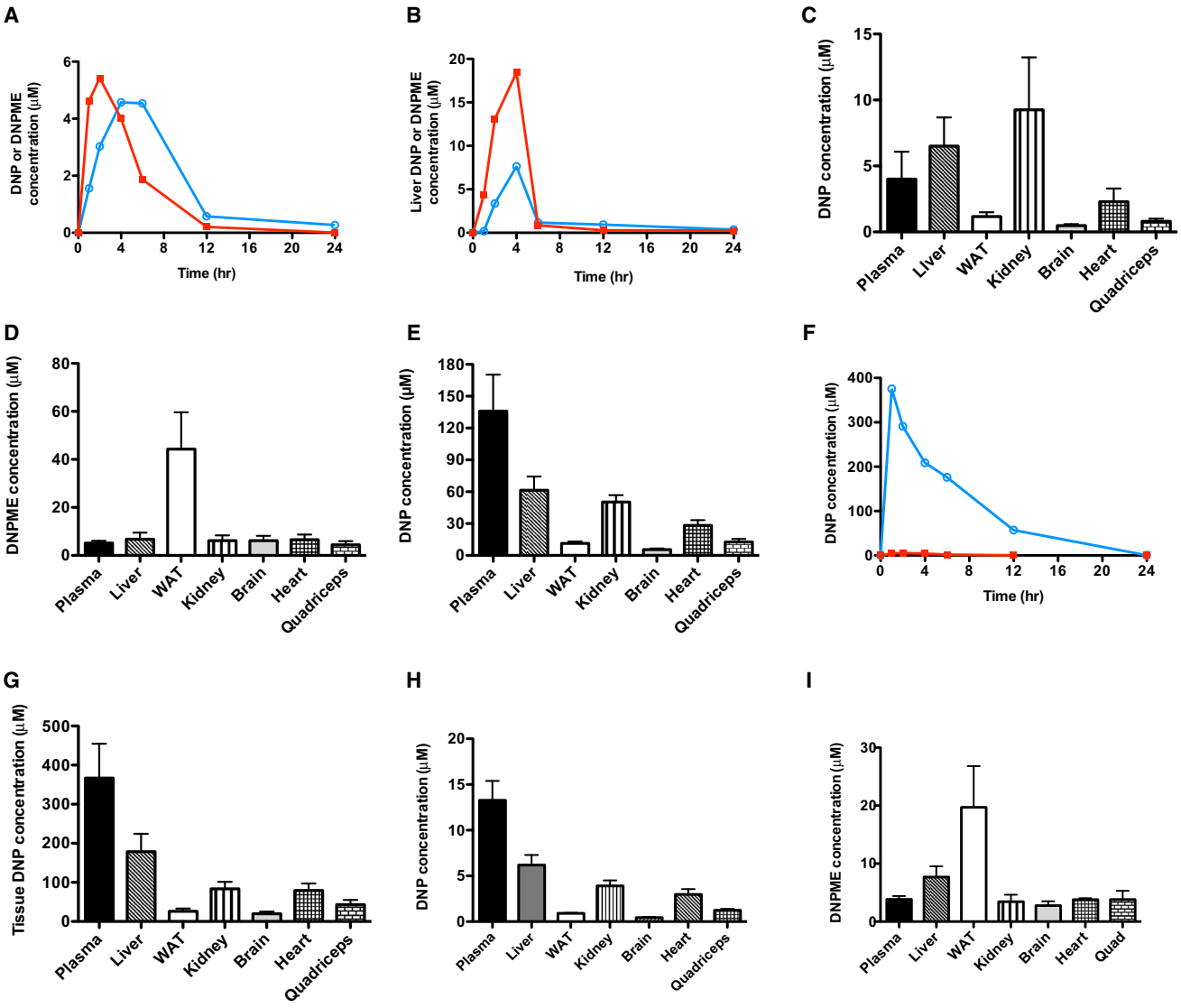

Figure 4. Plasma and Tissue Kinetics of DNP and DNPME Metabolism in Chow-Fed Sprague-Dawley Rats

(A) Plasma DNP and DNPME after an i.p. injection of DNPME (5 mg/kg). Red squares, DNPME; blue circles, DNP; each point represents one animal.

(B) Liver DNP and DNPME after an injection of DNPME (5 mg/kg). Red squares, DNPME; blue circles, DNP; each point represents one animal.

(C and D) Tissue DNP (C) and DNPME (D) 4 hr after an injection of DNPME (5 mg/kg).

(E) Tissue DNP 1 hr after an injection of DNP (5 mg/kg).

(F) Plasma DNP after an injection of DNP (25 mg/kg, blue circles) or DNPME (5 mg/kg, red squares). Each point represents one animal.

(G) Plasma and tissue DNP 1 hr after injection of DNP (25 mg/kg).

(H and I) Tissue DNP (H) and DNPME (I) after 7 days of daily DNPME injections (5 mg/kg). Unless otherwise noted, n = 4 per group. Data are expressed as mean ± SEM. See also Figure S4.

conversion to DNP or uncoupling by circulating DNP generated in the liver but released to the systemic circulation.

In order to gain further insight into why DNPME does not result in hyperthermia, whereas DNP does, we measured plasma and tissue levels of DNP and DNPME by liquid chromatography-tandem mass spectrometry (LC-MS/MS). We found that dosing rats with 5 mg/kg DNPME resulted in peak plasma DNP concentrations of ~5 μM and peak liver DNP concentrations of ~8 μM (Figures 4A and 4B). DNP concentrations in all tissues were below 10 μM, while DNPME accumulated in WAT, but not any other tissue (Figures 4C and 4D). In contrast, we found that the same dose of DNP (5 mg/kg) resulted in a peak plasma DNP concentration of ~120 μM and a peak DNP liver concentration of ~60 μM (Figure 4E). In order to determine how these plasma concentrations of DNP compare with toxic levels of DNP, we also examined plasma and liver concentrations of DNP at the lowest dose of DNP (25 mg/kg) where systemic toxicities are observed and found peak plasma DNP concentrations to be ~380 μM (Figures 4F and 4G). Importantly, a week of DNPME treatment resulted in tissue DNP and DNPME concentrations

similar to those following a one-time DNPME injection (Figures 4H and 4I). Further kinetics studies would be required to establish conclusively that the improved safety of DNPME versus DNP is purely the result of reduced DNP concentrations with DNPME treatment, but our data are consistent with this hypothesis. Our data also suggest that very low intracellular concentrations of DNP, which are more than 75-fold lower than toxic levels of DNP (380 μM), are sufficient to achieve significant liver mitochondrial uncoupling, resulting in reductions in ectopic lipid content and hepatic triglyceride export as well as reversing liver and muscle insulin resistance without resulting in hyperthermia and associated systemic toxicities.

In summary, we have demonstrated that DNPME can safely reverse hepatic steatosis, hypertriglyceridemia, and insulin resistance in a rat model of NAFLD without inducing hyperthermia and associated hepatic and systemic toxicities. We also found that DNPME reduces fasting plasma glucose concentrations and improves glucose tolerance in two rat models of T2D. Taken together, these data demonstrate the potential feasibility of dissociating the toxicity of DNP from its efficacy by altering the pharmacokinetics of DNP metabolism to treat the related epidemics of NAFLD, metabolic syndrome and type 2 diabetes.

EXPERIMENTAL PROCEDURES

General Experimental Procedures for Chemical Synthesis

Chemicals were obtained from commercial sources and used as received, unless noted otherwise. In particular, 2,4-dinitrophenol (DNP; 1) was purchased from MP Biomedicals, 2,4-dinitrophenyl methyl ether (DNPME; 2) from Alfa Aesar, and 1-chloro-2,4-dinitrobenzene-d3 (3) from C/D/N Isotopes. For detailed information on the synthesis and analysis of the unique compounds, please see the Supplemental Experimental Procedures.

Screening of Candidate Compounds

To screen candidate compounds, the ability of these compounds to raise oxygen consumption rates in vivo was assessed using the Extracellular Flux Analyzer (Seahorse Bioscience). Primary hepatocytes were isolated by the Yale Liver Center as previously described (Neufeld, 1997) and plated on a collagen-coated 24-well plate (Seahorse Bioscience). After a 6 hr incubation, cells were transferred to the Seahorse XF Analyzer for measurement of oxygen consumption rate. Basal oxygen consumption was measured, then sequential additions of DNP (positive control) or the candidate compounds raised the concentration of the putative uncoupler to 10, 100, 500, and 1,000 μM. Absolute oxygen consumption rates were normalized to the oxygen consumption rate measured before the first addition of uncoupler.

Animals

Male Sprague-Dawley and Zucker Diabetic Fatty rats were purchased from Charles River Laboratories, and male C57BL/6J mice were purchased from Jackson Laboratory. All protocols were approved by the Yale University School of Medicine Animal Care and Use Committee.

Unless otherwise noted, animals were fed normal chow (Harlan, diet 2018). Where specified, animals were fed 60% fat, safflower oil-based high-fat diet (Dyets). All animals had ad libitum access to water. Where specified, caloric intake was enriched by free access to 5% sucrose water. To measure caloric intake, the volume of water and weight of food consumed each day were measured, and calorie content was calculated using the known composition of each item. Rats underwent surgery under isoflurane anesthesia to place catheters in the jugular vein and internal carotid artery. All animals were allowed to recover for at least 1 week before any further experiments were performed.

To induce diabetes, rats were injected with 75 mg/kg nicotinamide and, following a 15 min wait, 60 mg/kg streptozotocin. Animals were allowed to recover for 3 days, and those with random plasma glucose between 150 and 350 mg/dl were used for further study. At this time, high-fat diet and sucrose water feeding was initiated. After 3 days of feeding, two weeks of daily DNPME or vehicle injections were begun.

Toxicity Studies

For the acute toxicity studies, rats were treated with an i.p. injection of various doses of DNPME. Rectal temperature was measured with a microprobe thermometer (Physitemp Instruments) at intervals up to 2 hr after injection of the drug. Rectal temperature was measured weekly in a separate group of rats injected daily with DNPME or vehicle for 6 weeks. A separate group of rats was injected with increasing doses of DNP or DNPME in 100% DMSO to determine the LD_{50}.

To assess renal and hepatic toxicity, a group of catheterized rats was treated with an i.p. injection of DMSO vehicle or varying doses of DNPME daily. After 5 days, the rats were sacrificed, and plasma was obtained from the intravenous catheter. The COBAS Mira Plus (Roche Diagnostics) was used to measure plasma alanine aminotransferase (ALT), aspartate aminotransferase (AST), and blood urea nitrogen (BUN), and creatinine was measured by LC-MS/MS. Daily creatinine clearance was measured by housing rats treated with DNPME or vehicle in metabolic cages for 24 hr, collecting the urine, and measuring urine creatinine by LC-MS/MS.

Histology Studies

Liver and kidney samples were prepared and stained with hematoxylin and eosin by the Yale Research Histology core and analyzed as described (Kleiner et al., 2005).

Glucose Tolerance Tests

Following an overnight fast, rats with a jugular venous line were injected with a 1 g/kg intraperitoneal bolus of 50% dextrose. Plasma glucose following the injection was measured enzymatically on the YSI 2700 SELECT Biochemistry Analyzer (YSI Life Sciences), and plasma insulin was measured by radioimmunoassay. Area under the curve (AUC) was measured from time point A to subsequent time point B according to the following formula:

$$AUC_{A\rightarrow B} = \frac{1}{2}\left(Plasma\ glc_A + Plasma\ glc_B\right) \times \left(Time_B - Time_A\right)$$

The total area under the curve was calculated by adding the area under the curve of all time periods. The insulin area under the curve was calculated in the same way.

Basal and Insulin-Stimulated Glucose Turnover Studies

Hyperinsulinemic-euglycemic clamps were performed, and basal and insulin-stimulated glucose turnover were measured using $[6,6]^2H_2$ glucose as previously described (Erion et al., 2013). To measure insulin-stimulated glucose uptake in heart and quadriceps muscle, [^{14}C]2-deoxyglucose was injected at the conclusion of the clamp, and tissues were processed as described previously (Samuel et al., 2007).

nProtein Kinase C Translocation

PKCε translocation in liver and PKCθ translocation in muscle from 6 hr fasted rats in the NAFLD treatment study were measured by western blot as reported by Choi et al. (2007).

Lipid Concentration Assays

TAG in liver and quadriceps muscle was extracted by the method of Bligh and Dyer (1959) and measured spectrophotometrically with triglyceride reagent (Diagnostic Chemicals Limited [DCL]). Liver and quadriceps DAG was extracted by homogenization in a buffer containing 20 mM Tris-HCl, 1 mM EDTA, 0.25 mM EGTA, 250 mM sucrose, 2 mM phenylmethylsulfonyl fluoride, and a protease inhibitor mixture (Roche). The cytosolic fragment was isolated from the supernatant after high-speed centrifugation for 1 hr. DAG and ceramide content was measured by LC-MS/MS (Yu et al., 2002). Liver triglyceride export was measured as we have described (Lee et al., 2011).

Measurement of Liver Glycogen Content

Hepatic glycogen content was assessed by amyloglucosidase digestion using the method of Passonneau and Lauderdale (1974).

Assessment of Plasma Metabolites, Adipocytokines, and Inflammatory Markers

Plasma concentrations of 12 inflammatory markers were measured by ELISA (QIAGEN). Adiponectin was measured by radioimmunoassay. Lactate was measured by COBAS and FGF-21 by ELISA (Millipore).

Assessment of Basal Metabolism in Mice

Mice were studied during daily i.p. injections of 5 mg/kg DNPME or vehicle. Comprehensive Animal Metabolic Monitoring System (Columbus Instruments) was used to measure oxygen uptake and carbon dioxide production, daily caloric intake and energy expenditure, respiratory exchange ratio, and activity.

Evaluation of Hepatic Flux Rates in Rats

To measure liver-specific flux through the TCA cycle, we performed a steady-state infusion of [3-^{13}C] lactate (5 min prime 120 μmol/[kg − min], 115 min continuous infusion of 40 μmol/[kg − min]) and [^{3}H] glucose (44 μmol/min). At 120 min, plasma and livers were isolated, and hepatic fluxes were measured by nuclear magnetic resonance (NMR) and LC-MS/MS as described in the Supplemental Experimental Procedures.

Measurement of Plasma and Tissue DNP and DNPME Concentrations

Plasma (10–100 μl) or tissue (~100 mg) was mixed with 2.0 ml prechilled chloroform/methanol (v/v: 2/1) containing 0.01% butylated hydroxytoluene (BHT) in 5 ml glass vials, then 250 μl water was mixed with 10 nmol DNP-D_3 and 10 nmol DNPME-D_6 as the internal standards. The mixtures were vortexed, centrifuged, and the bottom organic layer was carefully collected and dried with a steady stream of nitrogen gas, then reconstituted in 200 μl methanol for LC-MS/MS analysis. Analysis of DNP and DNPME was performed by LC-MS/MS using an Applied Biosystems 4000 QTRAP with Shimadzu ultrafast HPLC and electrospray ionization source with negative ion detection. The quantitative analysis of DNP was monitored in multiple reaction monitoring (MRM) mode with an ion pair (183.0/109.0). A Hibar LiChrosorb Analytical HPLC column (RP-C8, 4 × 125 mm, particle size 5 μM) (Merck KGaA) was used to separate DNP and DNPME using an isocratic flow of 15% 10 mM ammonium formate and 85% methanol/water (95/5). The retention time is ~4 min for DNP and ~7 min for DNPME.

Kinetics Studies

To evaluate the kinetics of DNP and DNPME, a 5 mg/kg dose of DNPME was injected at time zero. Rats were sacrificed at 1, 2, 4, 6, 12, and 24 hr to isolate the liver, and plasma was drawn through a venous catheter at each time point.

To compare tissue concentrations of DNPME and DNP with various injection protocols, separate groups of rats (n = 4 per group) were treated with 5 mg/kg DNPME, 5 mg/kg DNP, or 25 mg/kg DNP. The DNPME-injected rats were sacrificed 4 hr after the last injection, while the DNP-injected rats were sacrificed 1 hr after the last injection, which was found to represent the peak plasma concentrations of DNP with the respective injections.

Mitochondrial Respiration Studies

Isolated mitochondria from liver and brain of overnight-fasted rats were prepared (Andrews et al., 2008), and respiration was measured on the Seahorse XF Analyzer. Additional details may be found in the Supplemental Experimental Procedures.

Assessment of Tissue Energetics

To measure tissue ATP, ADP, AMP, NADH, and NAD^+ concentration, rats were sacrificed by decapitation, and metabolites of interest were extracted and measured by LC-MS/MS as described in the Supplemental Experimental Procedures.

Statistical Analysis

All data are expressed as mean ± SEM. Significance was determined using the two-tailed unpaired Student's t test or, if indicated, by the two-tailed paired Student's t test or ANOVA. Differences with a p value less than 0.05 were considered significant.

SUPPLEMENTAL INFORMATION

Supplemental Information includes Supplemental Experimental Procedures and four figures and can be found with this article online at http://dx.doi.org/10.1016/j.cmet.2013.10.004.

AUTHOR CONTRIBUTIONS

R.J.P and G.I.S designed the experimental protocols. R.J.P., X.-M.Z., H.-Y.L., D.P., V.B.P., D.Z., Y.R., M.J.J., and G.W.C. performed the studies. T.K. and D.A.S. contributed reagents. R.J.P., X.-M.Z., H.-Y.L., D.P., V.B.P., D.Z., Y.R., M.J.J., G.W.C., and G.I.S. analyzed the data. All authors contributed to the writing of the manuscript.

ACKNOWLEDGMENTS

We thank Jianying Dong, Mario Kahn, Blas Guigni, Bryce Perler, Jonathan Rajaseelan, Maria Batsu, and Kathy Harry for technical assistance. This work was supported by grants from the National Institutes of Health (R24 DK-085638, R01 DK-40936, R01 DK-49230, U24 DK-059635, P30 DK-45735, P30 DK-034989). The contents of this paper are solely the responsibility of the authors and do not necessarily represent the official view of NCRR or NIH.

Received: June 27, 2013
Revised: August 12, 2013
Accepted: October 4, 2013
Published: November 5, 2013

REFERENCES

Alves, T.C., Befroy, D.E., Kibbey, R.G., Kahn, M., Codella, R., Carvalho, R.A., Falk Petersen, K., and Shulman, G.I. (2011). Regulation of hepatic fat and glucose oxidation in rats with lipid-induced hepatic insulin resistance. Hepatology *53*, 1175–1181.

Andrews, Z.B., Liu, Z.-W., Walllingford, N., Erion, D.M., Borok, E., Friedman, J.M., Tschöp, M.H., Shanabrough, M., Cline, G., Shulman, G.I., et al. (2008). UCP2 mediates ghrelin's action on NPY/AgRP neurons by lowering free radicals. Nature *454*, 846–851.

Bligh, E.G., and Dyer, W.J. (1959). A rapid method of total lipid extraction and purification. Can. J. Biochem. Physiol. *37*, 911–917.

Choi, C.S., Savage, D.B., Abu-Elheiga, L., Liu, Z.-X., Kim, S., Kulkarni, A., Distefano, A., Hwang, Y.-J., Reznick, R.M., Codella, R., et al. (2007). Continuous fat oxidation in acetyl-CoA carboxylase 2 knockout mice increases total energy expenditure, reduces fat mass, and improves insulin sensitivity. Proc. Natl. Acad. Sci. USA *104*, 16480–16485.

Erion, D.M., Popov, V., Hsiao, J.J., Vatner, D., Mitchell, K., Yonemitsu, S., Nagai, Y., Kahn, M., Gillum, M.P., Dong, J., et al. (2013). The role of the carbohydrate response element-binding protein in male fructose-fed rats. Endocrinology *154*, 36–44.

Griffin, M.E., Marcucci, M.J., Cline, G.W., Bell, K., Barucci, N., Lee, D., Goodyear, L.J., Kraegen, E.W., White, M.F., and Shulman, G.I. (1999). Free fatty acid-induced insulin resistance is associated with activation of protein kinase C theta and alterations in the insulin signaling cascade. Diabetes *48*, 1270–1274.

Itani, S.I., Ruderman, N.B., Schmieder, F., and Boden, G. (2002). Lipid-induced insulin resistance in human muscle is associated with changes in diacylglycerol, protein kinase C, and IkappaB-alpha. Diabetes *51*, 2005–2011.

Kleiner, D.E., Brunt, E.M., Van Natta, M., Behling, C., Contos, M.J., Cummings, O.W., Ferrell, L.D., Liu, Y.C., Torbenson, M.S., Unalp-Arida, A., et al.; Nonalcoholic Steatohepatitis Clinical Research Network. (2005). Design and validation of a histological scoring system for nonalcoholic fatty liver disease. Hepatology *41*, 1313–1321.

Lee, H.-Y., Birkenfeld, A.L., Jornayvaz, F.R., Jurczak, M.J., Kanda, S., Popov, V., Frederick, D.W., Zhang, D., Guigni, B., Bharadwaj, K.G., et al. (2011).

Apolipoprotein CIII overexpressing mice are predisposed to diet-induced hepatic steatosis and hepatic insulin resistance. Hepatology *54*, 1650–1660.

Masiello, P., Broca, C., Gross, R., Roye, M., Manteghetti, M., Hillaire-Buys, D., Novelli, M., and Ribes, G. (1998). Experimental NIDDM: development of a new model in adult rats administered streptozotocin and nicotinamide. Diabetes *47*, 224–229.

Neufeld, D.S. (1997). Isolation of rat liver hepatocytes. Methods Mol. Biol. *75*, 145–151.

Passonneau, J.V., and Lauderdale, V.R. (1974). A comparison of three methods of glycogen measurement in tissues. Anal. Biochem. *60*, 405–412.

Petersen, K.F., Dufour, S., Befroy, D., Lehrke, M., Hendler, R.E., and Shulman, G.I. (2005). Reversal of nonalcoholic hepatic steatosis, hepatic insulin resistance, and hyperglycemia by moderate weight reduction in patients with type 2 diabetes. Diabetes *54*, 603–608.

Reed, M.J., Meszaros, K., Entes, L.J., Claypool, M.D., Pinkett, J.G., Gadbois, T.M., and Reaven, G.M. (2000). A new rat model of type 2 diabetes: the fat-fed, streptozotocin-treated rat. Metabolism *49*, 1390–1394.

Samuel, V.T., and Shulman, G.I. (2012). Mechanisms for insulin resistance: common threads and missing links. Cell *148*, 852–871.

Samuel, V.T., Liu, Z.-X., Qu, X., Elder, B.D., Bilz, S., Befroy, D., Romanelli, A.J., and Shulman, G.I. (2004). Mechanism of hepatic insulin resistance in non-alcoholic fatty liver disease. J. Biol. Chem. *279*, 32345–32353.

Samuel, V.T., Liu, Z.X., Wang, A., Beddow, S.A., Geisler, J.G., Kahn, M., Zhang, X.M., Monia, B.P., Bhanot, S., and Shulman, G.I. (2007). Inhibition of protein kinase Cepsilon prevents hepatic insulin resistance in nonalcoholic fatty liver disease. J. Clin. Invest. *117*, 739–745.

White, D.L., Kanwal, F., and El-Serag, H.B. (2012). Association between nonalcoholic fatty liver disease and risk for hepatocellular cancer, based on systematic review. Clin. Gastroenterol. Hepatol. *10*, 1342.e2.

Yu, C., Chen, Y., Cline, G.W., Zhang, D., Zong, H., Wang, Y., Bergeron, R., Kim, J.K., Cushman, S.W., Cooney, G.J., et al. (2002). Mechanism by which fatty acids inhibit insulin activation of insulin receptor substrate-1 (IRS-1)-associated phosphatidylinositol 3-kinase activity in muscle. J. Biol. Chem. *277*, 50230–50236.